Applied Surface Science 612 (2023) 155822

Contents lists available at ScienceDirect

Applied Surface Science

journal homepage: www.elsevier.com/locate/apsusc

Full Length Article

Density functional investigation of the interaction of H_2O with spinel $Li_{1-x}Mn_2O_4$ surfaces: Implications for aqueous Li-ion batteries

Gibu George [a], Sergio Posada-Pérez [a,*], Albert Poater [a], Miquel Solà [a]

[a] Institut de Química Computacional i Catàlisi and Departament de Química, Universitat de Girona, c/ Maria Aurèlia Capmany 69, 17003 Girona, Catalonia, Spain

ARTICLE INFO

Keywords:
Aqueous Li-ion batteries
Energy storage
Lithium manganese oxide
Oxygen evolution reaction
Density functional calculations

ABSTRACT

Aqueous lithium-ion batteries are receiving a lot of attention as large-scale energy storage technology owing to their low-cost, environmentally friendly, and safe behavior in comparison to commercial organic Li-ion batteries. However, aqueous batteries suffer fast degradation due to the interaction of water with electrodes. The O loss has often been claimed to deteriorate the electrode materials and the voltage window accessible for the cathode and anode is limited by aqueous electrolyte decomposition through O_2 evolution at the cathode and H_2 evolution at the anode. In this work, we use density functional theory simulations to unveil the behavior of spinel $Li_{1-x}Mn_2O_4$ as cathode material for aqueous Li-ion batteries exploring the $Li_{1-x}Mn_2O_4$ electrode deterioration at the surface level. The surface stability, O vacancy formation, interaction with water, and oxygen evolution reaction have been investigated at different Li concentrations, suggesting that a partially lithiated (011) surface can produce O_2 at low overpotential, and (001) termination can favor the presence of O and OOH intermediates anchored to the surface at 1.23 V, without generating O_2. Our work reveals the pros and cons of this material as a cathode for aqueous electrolytes and the importance of surface termination.

1. Introduction

Li-ion batteries (LIB) have clearly emerged in the last decades as the dominant battery technology and they are nowadays ubiquitous and the main energy storage source for small electronics [1] and electric vehicles [2]. However, one of the drawbacks of LIBs is the cost of the materials. One very appealing avenue to reduce the cost of LIBs is to replace the traditional organic electrolytes with water [3–6], which favors the Li conductivity and reduces the cost of the electrolyte salts, substituting the expensive organic salts with the inorganic ones like Li_2SO_4 and $LiNO_3$ [7,8]. In addition, aqueous LIBs are not only advantageous in terms of production cost, but also in terms of safety and toxicity, since the most common organic liquid electrolytes are flammable [9]. However, aqueous LIBs suffer from poorer cyclability and faster degradation in comparison to LIBs that use organic electrolytes. Many issues can explain the performance decay of aqueous LIBs such as the electrochemical stability of water electrolytes [10], owing to its decomposition to O_2 and H_2, which theoretically occurs at 1.23 V (vs. SHE) [11,12]. If these reactions occur, they are detrimental to the operation of aqueous batteries, as they degrade the electrolyte and build up gaseous pressure in the cell. Furthermore, water fraction can affect the electrode stability, promoting oxygen vacancy formation, metal dissolution, and phase transitions. These facts can accelerate the cathode degradation due to changes in the electronic structure [13–19]. However, the use of highly concentrated salts in the water electrolyte -the so-called "water-in salt" electrolytes- can increase the voltage window, reducing the O_2 and H_2 generation because of the Li^+ solvation, since there is not enough water to neutralize the lithium charge and it avoids the water-electrode interaction [20–22]. Nevertheless, further improvements are needed to limit the electrode degradation for future commercialization of aqueous batteries.

Owing to the demand for large-scale storage systems and the substitution of flammable, toxic, and expensive organic electrolytes, the research for stable electrode materials in an aqueous environment has received much attention [3,6,20,23–28]. In this sense, spinel $LiMn_2O_4$ has been extensively used as cathode material for Li-ion batteries, either using organic or aqueous electrolytes [29–38]. The major advantage of $LiMn_2O_4$ is its abundance and subsequent low cost. In fact, the first study using aqueous electrolytes carried out by Li and coworkers employed an anode of VO_2 and a cathode of $LiMn_2O_4$ [4], displaying the excellent performance of these water electrolytes although with a fast-fading capacity after a few cycles. The oxygen formation and oxygen loss during

* Corresponding author.
E-mail address: sergio.posada@udg.edu (S. Posada-Pérez).

https://doi.org/10.1016/j.apsusc.2022.155822
Received 15 September 2022; Received in revised form 17 November 2022; Accepted 20 November 2022
Available online 25 November 2022

delithiation process is commonly assumed to be the primary cause of lattice-oxygen evolution in lithium manganese oxide materials, either spinel (at high temperature) [16], rocksalt oxyfluoride [39], and Ni doped structures [40]. Nevertheless, it is worth mentioning that spinel $LiMn_2O_4$ has higher oxygen stability compared to layered ones [41]. Previous experimental studies (STEM) using spinel $LiMn_2O_4$ revealed that O deficiency near the surface can be associated with Li deficiency, with the subsequent decrease of oxidation state of Mn [42]. This fact promotes the formation of a thin surface layer where the formation of Mn_3O_4 was observed. In addition, irreversible O loss was observed after further cycles. Another experimental study at battery operation conditions (3.0–4.9 V vs Li^+/Li) shows that spinel $LiMn_2O_4$ has a stable bulk-level spinel structure, although it was detected an unusual phase transition to layered structure at surface region. These regions are closely related to the O loss, consequently to the degradation of electrochemical cycling performance of spinel $LiMn_2O_4$ [43]. As a positive point, it was experimentally and computationally proved that spinel crystal structures like $LiMn_2O_4$ have less tendency to host protons in the lattice structure in comparison to layered materials [44–47], and therefore, the cathode degradation and the hypothetic hindering of Li^+ insertion decreases. Understanding the mechanisms and processes for water-electrode interaction is essential to consciously designing cathode and anode materials for aqueous LIBs. In this sense, the processes that occur at the electrode–electrolyte interface are relevant since most of the electrode deterioration is found at the surface level, not at bulk [8]. The O vacancy formation and electrochemical water decomposition to oxygen, the so-called oxygen evolution reaction (OER), can be considered a good descriptor to elucidate the performance of electrodes in water electrolytes. Therefore, it is essential to explore the surface reactivity and reconstruction of electrode materials at different Li compositions to elucidate the possible effect of water and OER moieties on the surface structure, because it may affect the Li insertion [48,49] and battery performance.

Computational research has been essential during the last decades for a better understanding of the materials' performance, and it plays a key role in accurately predicting many properties of new materials for energy storage devices [50–52]. In this work, we have carried out a systematic and exhaustive computational investigation of the water interaction in the low-Miller indices of $LiMn_2O_4$ surfaces. The surface stability as a function of oxygen vacancies and Li^+/Li voltage, the water adsorption, and the mechanism of the OER have been studied to explore the capability of spinel $LiMn_2O_4$ to work as cathode material for aqueous Li-ion batteries. A good cathode for aqueous batteries must be an extremely bad catalyst for OER, i.e., it should have a high overpotential to avoid oxygen formation. Our findings shed new light on the interaction of $LiMn_2O_4$ surfaces with water, revealing the importance of surface termination, smoothing the path for the improvement $LiMn_2O_4$ cathode materials for LIBs.

2. Computational details and surface models

The periodic spin polarized DFT calculations were performed using the VASP code [53]. The Perdew-Burke-Ernzerhof (PBE) exchange–correlation functional [54] was used including the semi-empirical method of Grimme (D3) to describe the dispersion correction effects [55]. The surface models of $LiMn_2O_4$ modeled by Ramogayana and coworkers have been used in this work [56]. For the sake of comparison, we followed the same computational scheme. To better describe the strongly correlated 3*d* electrons of the Mn atoms, the DFT + *U* formalism was used following Dudarev method [57]. The selected U_{eff} value of 4.0 eV was chosen according to previous studies where the surface and bulk modelling were performed and is within the range of the value reported in Materials Project Database. The effects caused by the core electrons on the valence ones were described through the projected augmented wave (PAW) method of Blöchl [56] as implemented by Kresse and Joubert [59]. A Monkhorst–Pack grid of 5 × 5 × 1 k-points was used for the integration in the reciprocal space of all surfaces [60]. The threshold for electronic relaxation was less than 10^{-5} eV and relaxation of the atomic positions was allowed until forces acting on the atoms are always smaller than 0.01 eV $Å^{-1}$.

The METADISE code [61] was used to cut the bulk structure and to generate the non-polar surface terminations following the dipole method pioneered by Tasker [62]. The (0 0 1), (0 1 1), and (1 1 1) surface orientations were modeled. Initially, the cubic spinel of $LiMn_2O_4$ was fully optimized at GGA + U level and the studied surface terminations were generated considering the stoichiometric structure, that contains 8Li, 16 Mn, and 32O atoms. The (0 0 1), (0 1 1), and (1 1 1) surface terminations belong to Tasker type 3 surfaces, where the slab model alternates charged planes stack in a sequence that produces a dipole moment perpendicular to the surface. The surface reconstruction is therefore required in order to cancel the dipole moment. Take for instance the (0 0 1) termination of $LiMn_2O_4$, the surface can be reconstructed through moving half of the ions with the same charge from the top to the bottom of the slab. The Li terminated surface is the lowest in energy for (0 0 1), in agreement with previous works [63–66]. With respect to (0 1 1) surface, the Li/Mn/O termination is the most stable according to Ramogayana and coworkers [56], in agreement as well with the previous computational studies [63–66]. Regarding (1 1 1) terminations, all the studies determined that Mn terminated surface is the lowest energy before the reconstruction process. Nevertheless, the works of Karim [63] and Benedeck [64] revealed, using molecular dynamics simulations, a surface reconstruction based on the external Mn by subsurface Li exchange, forming the inverse spinel $LiMn_2O_4$. In this case, the coordination of Mn increase, stabilizing the surface, which is Li terminated. In this work, we have used the non-reconstructed (1 1 1) termination. First of all, the partial formation of inverse $Li_{1-x}Mn_2O_4$ was experimentally observed at high voltages (5.3 V vs Li^+/Li) [67], which is not commonly reached during battery operations using water electrolytes. Secondly, the adsorption of OER moieties occurs normally on top of Mn atoms, being the interaction with O-surface atoms very weak, even repulsive. Thus, we decided to employ the non-reconstructed model. It is important to remark that this choice can imply larger binding energies for (1 1 1) surface, although as is presented in the results section, it is not relevant for the final remarks. In addition, it is worth mentioning that the synthetic conditions of the cathode material clearly determine the surface structure and stoichiometry, and consequently, the surface energies. In this work, we use the perfect models of $LiMn_2O_4$ considering the surface models optimized in previous works [56,63–66], and evaluating the surface energy (see below) as function of the voltage.

For each surface termination, three models with different Li^+ concentrations were considered to mimic the effect of the charge/discharge process on battery operations. The delithiated (0 0 1) and (0 1 1) contain seven and five Li atoms, whereas two and four Li atoms were removed from (1 1 1) orientation. This is because the surface structure; the (0 0 1) and (0 1 1) contain one Li atom in the most external layers (top and bottom) and two Li in the most internal layers. Then, we have removed the most external Li atom for the first delithiated configuration ($Li_7Mn_{16}O_{32}$) and the following two atoms for the most internal layer ($Li_5Mn_{16}O_{32}$). However, the (1 1 1) contains two Li atoms *per* layer, and the delithiated surface models have lost two Li at a time ($Li_6Mn_{16}O_{32}$ and $Li_4Mn_{16}O_{32}$). The delithiation and O vacancy formation was modeled by removing the most external atoms allowing the atomic relaxation and the subsequent surface reconstruction.

The surface Gibbs energy (hereafter, surface energy) has been computed following equation (1), considering the difference in the Gibbs energy between the bulk material and the slab model per unit area,

$$\gamma^{clean} = \frac{1}{2S}\left[G^{slab} - G^{bulk}\right] \quad (1)$$

where S is the total surface area, G^{slab} is the Gibbs energy of the

surface and G^{bulk} is the Gibbs energy of the bulk. The Gibbs energies were approximated by the DFT total energy of the clean surface and $LiMn_2O_4$ bulk, i.e., the entropic contribution has been neglected. To take into account the effect of delithiation and oxygen vacancies, equation (1) must be adapted considering the species in excess or shortage and taking into account the effect of chemical potential for the different species μ_i:

$$\gamma^{clean} = \frac{1}{2S}\left[G^{slab} - G^{bulk} - \sum_i \Delta N_i \mu_i\right] \quad (2)$$

where ΔN_i is the variation of the number of atoms for the species i from the surface to the bulk. Equation (2) allows to represent the surface energy as a function of the applied voltage, since the μ_{Li} can be related to the voltage following equation (3):

$$V = -\frac{\mu_A^{cathode} - \mu_A^{anode}}{zF} = -\frac{\mu_A - \mu_A^{ref}}{zF} \quad (3)$$

where A represents Li^+, F is the Faraday constant, and z is the number of electrons. Thus, applied voltage modifies the μ_{Li} and subsequently, the surface energy, which led to investigating the most favorable surface slab depending on the applied voltage.

The reaction mechanism of OER generally proceeds in four steps (equations 4–7) [68,69],

$$H_2O\ (l) + * \rightarrow *OH + H^+ + e^- \quad (4)$$

$$*OH \rightarrow *O + H^+ + e^- \quad (5)$$

$$H_2O\ (l) + *O \rightarrow *OOH + H^+ + e^- \quad (6)$$

$$*OOH \rightarrow O_2 + * + H^+ + e^- \quad (7)$$

where * represents the bare surface of $LiMn_2O_4$ and *OH, *O, and *OOH represents the adsorbed species on $LiMn_2O_4$. We have followed the so-called computational hydrogen electrode approach proposed by Nørskov and coworkers [70]. This approach assumes that the energy of $H^+ + e^-$ can be computed as half of the Gibbs energy of the H_2 molecule at 0 V vs SHE at 1 bar and 1 M activity. The absolute potential of SHE is 4.44 ± 0.02 V at 25 °C but its potential is set to be zero in order to serve as the reference of zero potential at all temperatures. The Gibbs energy of each reaction can be obtained by exploring the adsorption of OH, O, and OOH moieties on the corresponding surfaces. Therefore, the cathode performance as active or inactive catalysts depends on the binding energies of these moieties on the catalyst's active sites [71]. Equations 8–11 show how to compute the Gibbs energies of each reaction step at standard conditions. The U_{SHE} term is the electrode potential referred to SHE and e is the number of electrons. The overpotential is calculated as the difference between the potential required to thermodynamically allow the reaction and the equilibrium potential of OER, 1.23 V [67]. The vibrational frequencies of the adsorbed reactants have been calculated to account for the zero-point energy and the entropic effects. The approach considers the effect of liquid water although the interaction of water with the surface is neglected. For further details, look up the pioneering and review works in references [68–70].

$$\Delta G_1 = \Delta G_{*OH} + 1/2\Delta G_{H2} - \Delta G_* - \Delta G_{H2O} - eU_{SHE} \quad (8)$$

$$\Delta G_2 = \Delta G_{*O} + 1/2\Delta G_{H2} - \Delta G_{*OH} - eU_{SHE} \quad (9)$$

$$\Delta G_3 = \Delta G_{*OOH} + 1/2\Delta G_{H2} - \Delta G_{*O} - \Delta G_{H2O} - eU_{SHE} \quad (10)$$

$$\Delta G_4 = \Delta G_* + 1/2\Delta G_{H2} + \Delta G_{O2} - \Delta G_{*OOH} - eU_{SHE} \quad (11)$$

It is important to remark that during battery operation conditions the electrode–electrolyte interaction can generate an interphase. The formation of the interphase is not trivial and the cathode interfacial stability during charge–discharge process is found to be far more complex than purely thermodynamic/phase diagram approaches [71]. Therefore, to consider only the adsorption of OH, O, and OOH species on perfect modeled surfaces is a simplified but useful model to evaluate the OER, even though the interphase formation is not considered. On the other hand, $LiMn_2O_4$ is not a passive electrode, since the Li content will change as the applied voltage varies. One must take into account that the overpotential required to produce the OER may imply the delithiation of the surface, and therefore, the real Li content at this particular overpotential may no longer correspond to the calculation performed under the initial Li-content on the surface. In other words, if the delithiation process occurs at lower voltages than the overpotential, the OER will not occur at this Li concentration.

3. Results

3.1. O_{vac} formation and stability of $LiMn_2O_4$ surfaces

The variation of the surface energy from full to partially lithiated $LiMn_2O_4$ (001), (011), and (111) surfaces has been investigated as a function of the oxygen content and the Li^+/Li voltage. The latter controls the Li^+ content on the cathode material during the charge/discharge process of the battery. In this work, $\Delta\mu_{Li}$ is defined as the difference between the chemical potential of Li and its reference chemical potential at 0 K, i.e., the DFT energy of Li bulk (-1.91 eV). We assumed that during battery operations the temperature and pressure is fixed and then, we considered a constant chemical potential for O and Mn species, being the voltage the external factor that can modify the surface energy. Note that the higher the voltage, the energetically more favored the delithiation is. The delithiation process may imply the surface reconstruction with the subsequent formation of oxygen vacancies, which may affect the performance of the cathode. On the other hand, one should consider the differences between organic and aqueous electrolytes with respect to the interaction with the cathode material. With respect to organic electrolytes, a good cathode material favors the formation of a protective solid-electrolyte interphase (SEI) on the surface of the cathode material after the electrolyte decomposition [72]. However, the dissociation of aqueous electrolyte cannot form traditional SEI. In this case, the key is the formation of a solid–liquid interphase, as it was shown using $LiFePO_4$ electrode that promote the Li desolvation during charge discharge process [73,74]. To enhance the fast kinetics of charge/discharge process in aqueous electrolytes, the cathode surface should maintain their structure after the formation of Li vacancies, without significant reconstruction. The surface reconstruction may result in a redistribution of the surface atoms, occupying the Li vacancy site and hindering the Li reinsertion.

Fig. 1 shows the surface energy at different O compositions as a function of Li^+/Li voltage. With respect to (001) termination, it is clearly observed that the formation of oxygen vacancies does not stabilize the surface energy. The O_{vac}-free configurations (blue lines) are the most stable independently of the amount of Li. Below 3.3 V vs. Li^+/Li the full lithiated surfaces without oxygen vacancies are the most stable configuration. Our simulations predict the surface delithiation above 3.3 V ($Li_{0.875}Mn_2O_4$) and 4.9 V ($Li_{0.625}Mn_2O_4$). In comparison to the other surface terminations, the delithiation process begins at larger voltages, which is related to the large stability of (001) termination. One can observe that the surface energy is lower with respect to (011) and (111) terminations and this is related to the Mn coordination. In the case of (001), the most external Mn atoms are 5-fold coordinated (they lose one of the O atoms while the internal O atoms are octahedrally coordinated). Nevertheless, in the case of (011) surface, the most exposed Mn atoms are 4-fold coordinated. The (111) surface only contains one Mn atom on the most exposed surface due to the surface reconstruction, which is required to redistribute the charge and generate stoichiometric slabs [58]. The rest of Mn atoms are octahedrally coordinated. Clearly, metal coordination affects surface energy [17,75]. For this reason the exchange of the most exposed Mn atom by a Li atom (inverse spinel configuration) is energetically favored.

Going into details about (011) termination, configurations without

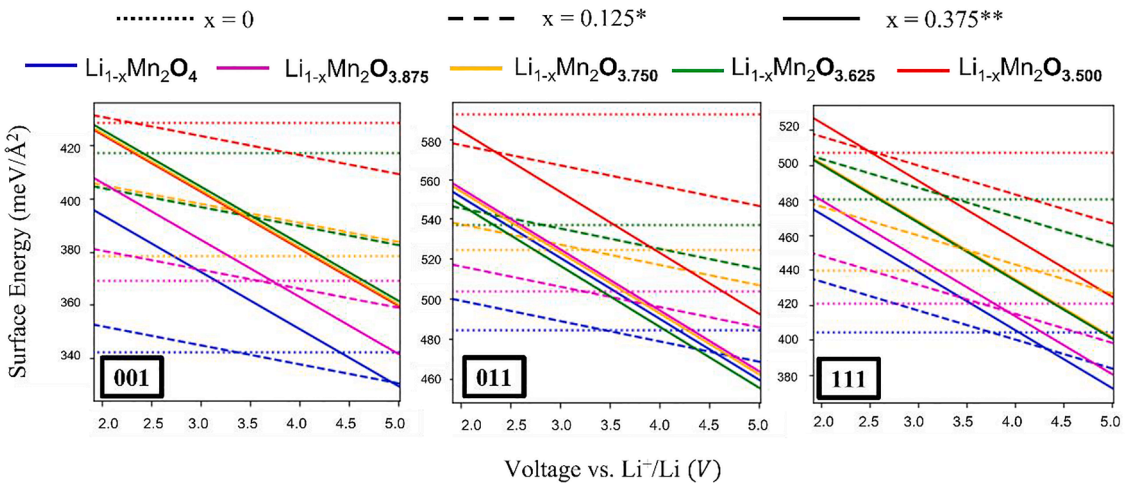

Fig. 1. Surface energy (meV/Å^2) as a function of the voltage vs. Li^+/Li for the three different surface terminations of $Li_{1-x}Mn_2O_4$ with different Li^+ content. Dotted, dashed, and solid lines represents $LiMn_2O_4$, $Li_{0.875}Mn_2O_4$, and $Li_{0.625}Mn_2O_4$ configurations respectively. The different colors represent different concentrations of O_{vac} on the most external surface layer. *For (1 1 1) termination, the stoichiometry is $Li_{0.75}Mn_2O_4$. **For (1 1 1) termination, the stoichiometry is $Li_{0.5}Mn_2O_4$.

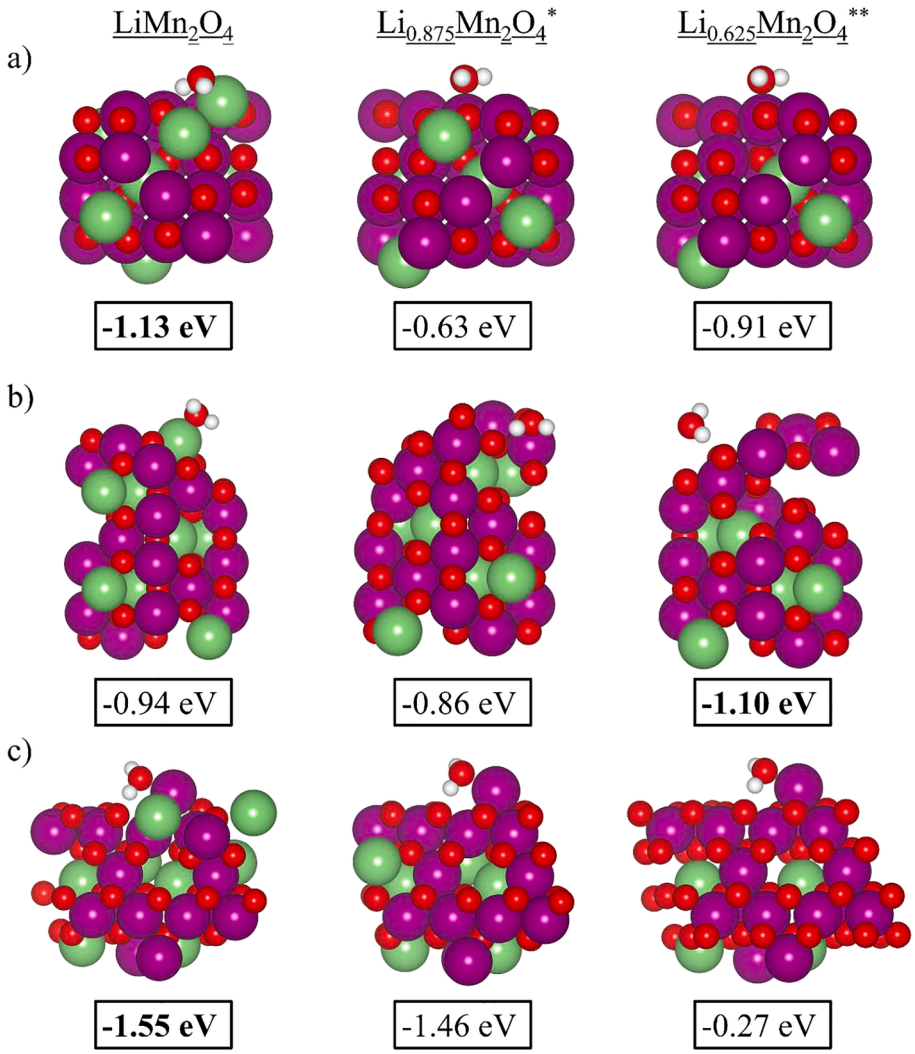

Fig. 2. Sketches of the lowest energy configurations of water adsorbed on $Li_{1-x}Mn_2O_4$ a) (0 0 1), b) (0 1 1), and c) (1 1 1) surfaces. Green, violet, red, and white colors represent Li, Mn, O, and H atoms respectively. *For (1 1 1) termination, the stoichiometry is $Li_{0.75}Mn_2O_4$. **For (1 1 1) termination, the stoichiometry is $Li_{0.5}Mn_2O_4$ (for interpretation of the references to colour in this figure legend, the reader is referred to the web version of this article).

oxygen vacancies are energetically favored at high Li content. Nevertheless, at 4.3 V the delithiation process favors the oxygen loss. As is plotted in Fig. 1 (center), $Li_{0.625}Mn_2O_{3.625}$ configuration (green) is lower in energy with respect to the configuration without oxygen vacancies. For this system, the most exposed Mn atoms are 4-fold coordinated and the Mn on the subsurface have a coordination of 5. Moreover, the $Li_{0.625}Mn_2O_{3.750}$ and $Li_{0.625}Mn_2O_{3.875}$ structures (orange and magenta, respectively) are very close in energy to the configuration without oxygen vacancies, $Li_{0.625}Mn_2O_4$. We observed the formation of O_2 during the reconstruction process for $Li_{0.625}Mn_2O_{3.750}$ which indicated that (0 1 1) termination may promote oxygen formation during the charge/discharge process.

Finally, the (1 1 1) cut follows the same tendency observed for (0 0 1) termination, where configurations without oxygen vacancies are energetically more stable. Below 3.7 V, the full lithiated surface is the most stable, the $Li_{0.875}Mn_2O_4$ is favored between 3.7 and 4.2 V, and $Li_{0.625}Mn_2O_4$ above 4.2 V. It is important to remark that $Li_{0.625}Mn_2O_{3.875}$ is very close in energy to the configuration without vacancies which may promote the oxygen vacancy formation at voltages superior to 4.3 V. In summary, the surface energy analysis reveals that is not energetically expensive to generate oxygen vacancies at partially delithiated $LiMn_2O_4$ (0 1 1) and (1 1 1) surfaces, especially when the Mn coordination is not 6-fold.

3.2. Water adsorption on $Li_{1-x}Mn_2O_4$ surfaces

The interaction with water has been investigated by adsorbing the water molecule on several sites of the three surface terminations of $LiMn_2O_4$ considering the different Li content. The configurations with the largest binding energies are illustrated in Fig. 2, and Table S1 collects the water adsorption energy on different adsorption sites for all the tested surfaces. For (0 0 1) surface, the largest binding energy is predicted for the full lithiated stoichiometry (−1.13 eV). In this case, the water molecule is chemisorbed with the oxygen atom bonded to the most exposed Li and the hydrogen atoms pointing to the oxygen of the surface. When the oxygen atom is placed on top of the Mn, the adsorption energy is weaker (−0.63 eV, see Table S1). The partially lithiated configurations do not contain the exposed Li atom and then the water is adsorbed on top of the Mn atoms, as it is depicted for $Li_{0.875}Mn_2O_4$ and $Li_{0.625}Mn_2O_4$. The adsorption energy decreases to −0.63 and −0.91 eV, respectively. These differences may be related to the Li and Mn coordination. The internal Li atoms are tetrahedrally coordinated and the interaction with H_2O is not favored, while the exposed Li atom on the most external layer is 3-fold coordinated. Thus, the water adsorption is indeed favored on top of the most exposed Li atom.

One can expect that the adsorption on surfaces with higher surface energy may imply larger binding energies and possible surface reconstructions. However, it is not observed for (0 1 1) terminations, where similar binding energies were found in comparison to (0 0 1) termination. For the full lithiated configuration, the H_2O is adsorbed, again, on top of the most external Li atom (−0.94 eV). We found a degenerated adsorption site (−0.94 eV), where the H_2O molecule is placed on the first surface layer, adsorbed on the subsurface, with the oxygen bonded to one of the Mn atoms (1.98 Å) and the hydrogen atoms aimed at oxygen surface atoms (1.74 Å). The latter adsorption site is the most favored (−0.86 eV) for $Li_{0.875}Mn_2O_4$ configuration. The displacement of the H_2O upwards to be placed on top of the most external Mn atom comes with an energy cost of 0.22 eV, and thus, our simulations suggest that H_2O prefers to be adsorbed on the subsurface. The largest binding energy is found for $Li_{0.625}Mn_2O_4$ configuration, where the H_2O is adsorbed perpendicular to the surface forming an H-O bond with the surface. This geometry is 0.49 eV favored over the structure containing H_2O inside the most exposed surface layer.

Finally, the largest binding energies were found on (1 1 1) termination. Of course, it can be related with the fact that Mn terminated surface is higher in energy than the reconstructed surface. The adsorption with low-coordinated Mn atom implies higher binding energy of water molecules. Independently of the Li content, the H_2O is adsorbed perpendicular to the surface with one of the hydrogen atoms bonded to one of the O atoms of the surface, with an H-O distance between 1.50 and 1.70 Å, and the oxygen atom very close to the exposed, and consequently less coordinated, Mn atom (2.17 Å). A large binding energy was found for the full lithiated configuration. One can observe that the adsorption energy for $Li_{0.50}Mn_2O_4$ surface is weak in comparison to more lithiated structures. This is because during the optimization process, one of the O–H bonds of H_2O is broken, forming an OH moiety, with the free H bonded to one of the surface oxygen atoms. The binding energy of this system, is −1.36 eV, taking the energy of the water molecule as a reference. It occurs for all the tested systems in this surface termination, except for the system illustrated in Fig. 2c, with a binding energy of −0.27 eV. The same situation was obtained for full lithiated surface, although in this case, the energy difference between the H_2O and the *OH + *H adsorption is only 0.14 eV favorable to the cleavage moiety.

3.3. Oxygen evolution reaction (OER) on $Li_{1-x}Mn_2O_4$ surfaces

The OER has been investigated on the three different surface terminations of $Li_{1-x}Mn_2O_4$. The OER mechanism has been studied by adsorbing the *OH, *OOH, and *O moieties on different surface sites of bare slabs. First of all, it is important to remark that the adsorption of OH, OOH, and O moieties occur on top of the most external Mn surface atoms. Initially, the moieties were adsorbed as well on top of the oxygen atoms, although the binding energy is weaker, and in some cases, the moiety is displaced towards the top Mn site during the optimization process. This fact is directly related to the Mn coordination. As it was previously commented, the most exposed Mn atoms are less coordinated with respect to the most internal. Therefore, the adsorption of the moieties on Mn atoms increases the Mn coordination number and stabilizes the surface.

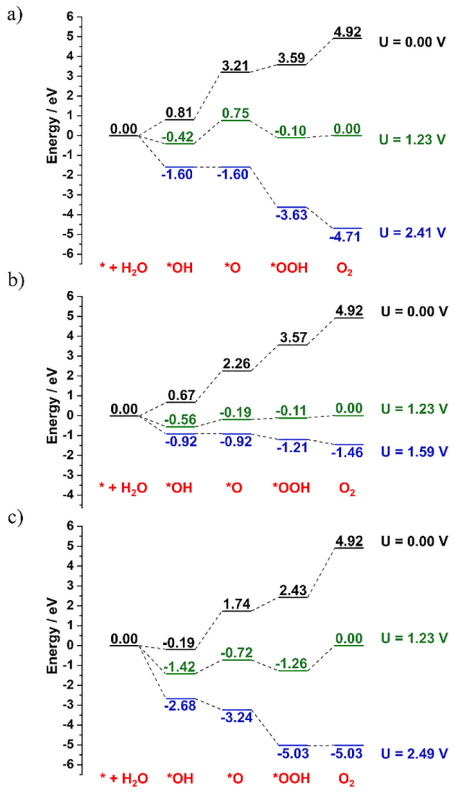

Fig. 3. Reaction mechanism of OER on bare $Li_{0.625}Mn_2O_4$ a) (0 0 1), b) (0 1 1), and bare $Li_{0.5}Mn_2O_4$ (1 1 1) surfaces.

We have computed the thermodynamic energy profile at 0 V, 1.23 V, and at the voltage where the reaction is thermodynamically feasible. Fig. 3 illustrates the OER mechanism plots for all the surface terminations with the lowest amount of Li. The plots of the full and high lithiated surfaces are provided in the Supporting Information (Figures S1-S3). We have observed that the OER is not feasible at high Li content. Note that the voltage at which the OER occurs, according to DFT simulations, is higher than the delithiation voltage of these surfaces, i.e., highly lithiated $Li_xMn_2O_4$ surfaces will lose lithium before catalyzing the OER. Therefore, the Li-content would change at the overpotential required to perform the OER, and the reaction mechanism does not correspond to the initial surface (see Figures S1-S3). In these cases, at high Li concentrations, the cathode material does not maintain the same Li content at the beginning and at the end of the reaction, which indicate that this particular Li concentration avoids the O_2 formation.

Focusing on (001) termination, the cleavage of OH moiety is the most energetically demanding step. The sketches of all intermediate species are reported in Figure S4. According to our simulations, the OER can occur at voltages from 2.28 to 2.70 V vs SHE (5.32–5.74 V with respect to Li^+/Li voltage). These results imply an overpotential higher than 1 V in the most favorable case (see Table 1). This voltage window is not reachable during battery operations. At high Li-content, the delithiation occurs before, and at low lithiated configurations, the overpotential is higher than the cathode stability. Thus, the (001) termination is not a good catalyst for OER neither full nor partially lithiated surface, which implies that (001) termination of $LiMn_2O_4$ does not contribute to aqueous electrolyte degradation. The *O formation is again the rate-limiting step for (011) termination. As reported in Table 1, a slightly lower but still larger overpotential is required for high Li content (011) surfaces. However, a very low overpotential is predicted (0.36 and 0.57 V) for the OER using the $Li_{0.625}Mn_2O_4$ and $Li_{0.875}Mn_2O_4$ (011) configurations, respectively. For the latter, a voltage of 1.80 V (4.85 V vs Li^+/Li) is predicted for the O_2 generation, only 0.15 V higher than the voltage predicted for the delithiation process (see Figure S2). Thus, both processes are competitive. With respect to $Li_{0.625}Mn_2O_4$ configuration, a voltage of 1.59 V vs SHE is required (4.63 V vs Li^+/Li). Thus, the delithiation of $LiMn_2O_4$ (011) can promote the OER reaction with the subsequent electrolyte and cathode degradation. Moreover, DFT simulations suggest that lower Li concentration, lower overpotential, which may indicate the facility to produce O_2 at higher voltages. It is worth mentioning that this surface termination is higher in energy with respect to the other surface terminations explored in this work, which it will be the less exposed surface termination at the electrode–electrolyte interphase. With respect to (111) orientation, the rate-limiting step is the O_2 formation independently of the Li concentration (see Figure S3). One can observe (Fig. 3c and Figure S3) that a high overpotential is required to generate O_2, i.e., it is not a suitable catalyst. One can expect that Mn-terminated surface, being higher in energy with respect to the reconstructed (111) termination [64,65], would be favored to OER reaction. Nevertheless, this surface termination is not predicted to be active, even though the low-coordinated Mn is a very active catalytic site. In contrast to (001) and (011), the *OH bond cleavage with the subsequent *O generation is not that energy demanding, and an overpotential between 0.70 and 0.81 V is required. Even though the O_2 production is not suggested by our simulations, the deposition of atomic oxygen is predicted at voltages around 5 V vs Li^+/Li.

Owing to the strong Mn-OH interaction, the OER has been further investigated considering the coverage of one OH moiety as it was carried out in other works using Pt as a catalyst [76]. In our case, the OH has been adsorbed on top of Mn atoms. Then, the following OH, OOH, and O moieties have been placed on the different sites of $LiMn_2O_4$ surfaces that contain one OH moiety adsorbed. To facilitate the comparison between the OER mechanism on bare or OH-covered surfaces, the latter ones have been indexed adding OH before the surface termination. The reaction mechanism of low lithiated surfaces of the three studied terminations are exhibited in Fig. 4, and Figures S5-S7 illustrate the plots for the different Li concentration. Table 2 reports the overpotential values together with the rate-limiting step of the reaction. Analyzing the results

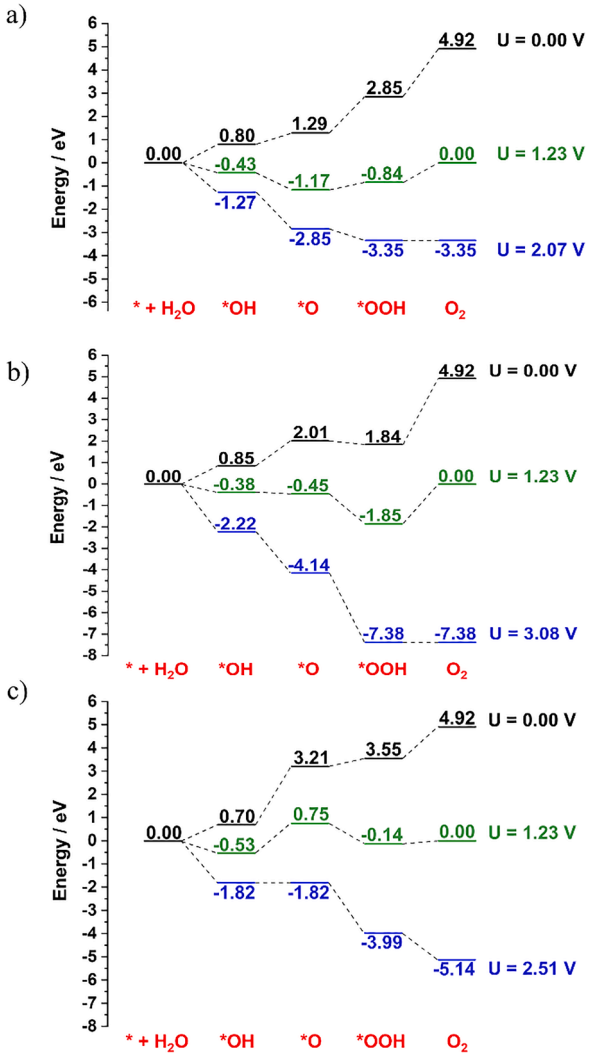

Fig. 4. Reaction mechanism of OER on OH-covered $Li_{0.625}Mn_2O_4$ a) (001), b) (011), and OH-covered $Li_{0.5}Mn_2O_4$ (111) surfaces.

Table 1
Overpotential (V) and rate-limiting step (RLS) of OER for bare $Li_{1-x}Mn_2O_4$ surfaces. Values indexed with "*" shows that the delithiation requires lower voltage than the overpotential, while "**" indicates competitive processes.

	(001)		(011)		(111)	
	Overpotential (V)	RLS	Overpotential (V)	RLS	Overpotential (V)	RLS
$LiMn_2O_4$	1.05*	*O formation	0.95*	*O formation	1.26*	O_2 formation
$Li_{0.875}Mn_2O_4$	1.48*	*O formation	0.57**	*O formation	1.05*	O_2 formation
$Li_{0.625}Mn_2O_4$	1.18	*O formation	0.36	*O formation	1.26	O_2 formation

Table 2
Overpotential (V) and rate-limiting step (RLS) of OER for OH-$Li_{1-x}Mn_2O_4$ surfaces. Values indexed with "*" shows that the delithiation requires lower voltage than the overpotential.

	(001)		(011)		(111)	
	Overpotential (V)	RLS	Overpotential (V)	RLS	Overpotential (V)	RLS
$LiMn_2O_4$	1.53*	O_2 formation	1.39*	O_2 formation	0.97*	*O formation
$Li_{0.875}Mn_2O_4$	1.14*	O_2 formation	1.39*	O_2 formation	1.18*	*O formation
$Li_{0.625}Mn_2O_4$	0.84	O_2 formation	1.85	O_2 formation	1.28	*O formation

for OH–(001) termination, there are remarkable differences with respect to bare (001), especially at the lowest Li concentration. For $LiMn_2O_4$ the rate-limiting step is the *OOH formation with an overpotential of 1.53 V although as in bare surface, the *OH bond cleavage is energetically demanding as well. For $Li_{0.875}Mn_2O_4$ the rate-limiting step is the *OOH dissociation, the last step prior the O_2 formation. The overpotential is 1.14 V and again, as observed in Figure S5, the *OH bond cleavage is energetically demanding. For both configurations, the delithiation process is favored over O_2 formation. The most interesting results were found for $Li_{0.625}Mn_2O_4$ as illustrated in Fig. 4a. The rate-limiting step of the reaction is the *OOH dissociation, with an overpotential of 0.84 V. Although the overpotential required for O_2 production is still large, it is the first system where the OH moiety can be dissociated (*OH→*O) at equilibrium reaction voltage (1.23 V). Note that in Fig. 3 and Figures S1-S3, for bare termination surfaces without OH-coverage, the *OH bond cleavage is not thermodynamically feasible at 1.23 V in any surface terminations independently of the Li content. However, the presence of two adsorbed *OH moieties can facilitate the formation of atomic oxygen on the most exposed surface layer. Even though the OER has a predicted overpotential of 0.84 V, our simulations suggest that the OH-coverage may facilitate the *OH dissociation and *O deposition. Nevertheless, the tendency of our results for OH–(001) surface indicated less Li content in the cathode, lower overpotential required to produce O_2, which is not a promising trend for the performance of aqueous LiBs.

Focusing on OH–(011) termination, one can observe that it follows the same tendency that OH–(001). An overpotential of 1.39 V is predicted for OH-$LiMn_2O_4$ and OH-$Li_{0.875}Mn_2O_4$ configurations, and unexpectedly, an overpotential of 1.85 V is observed for $Li_{0.625}Mn_2O_4$ surface. It is in opposition to the OER mechanism predicted on bare surfaces, where $Li_{0.625}Mn_2O_4$ (011) was suggested as a good catalyst, i.e., bad cathode material. In this case, the delithiation of $Li_xMn_2O_4$ material is favored because it implies low voltages than the required overpotential for OER. Nevertheless, one must point out, that again, as observed for OH–(001) termination, the rate-limiting step of the reaction is the *OOH rupture and the subsequent O_2 formation, although the reaction mechanism illustrated in Fig. 4b reveals that the formation of *O and *OOH moieties is favored at the equilibrium potential at low lithiated configuration. In other words, DFT simulations do not predict the O_2 generation even though it is suggested that the surface is covered by all the intermediate moieties even at 1.23 V. It clearly indicates water decomposition. Therefore, the presence of *OH moieties on the surface increases the overpotential required to generate O_2 although it favors the formation of the intermediates adsorbed on lithium manganese oxide surface. The rate limiting-step for OH–(111) surface is the OH bond cleavage, with an overpotential of 0.97, 1.18, and 1.28 V for $LiMn_2O_4$, $Li_{0.75}Mn_2O_4$, and $Li_{0.5}Mn_2O_4$ configurations, respectively. Thus, as less lithiated the surface is, the higher the overpotential. It is worth mentioning that the most demanding step on clean surface was the O_2 formation. Our simulations predict that this surface termination does not allow the water decomposition at equilibrium voltage and the generation of reaction intermediates, which is *a priori* essential for the performance of $LiMn_2O_4$ as cathode for aqueous batteries.

4. Conclusions

Density functional simulations have been used to investigate the interaction of water with $LiMn_2O_4$ surfaces – (001), (011), and (111) – with the goal to explore its pros and cons as cathode material for aqueous Li-ion batteries. The surface energy at different Li content as a function of Li^+/Li voltage was computed, revealing that (001) termination does not have the tendency to form oxygen vacancies, showing that the surface reconstruction is minimal. Nevertheless, our simulations suggest that surfaces with oxygen vacancies are lower in energy at low lithiated (011), predicting the O_2 formation. The binding energy of water was explored, showing moderate-large interactions with the $LiMn_2O_4$ surfaces. The most relevant result was found for partially lithiated (011), where H_2O is adsorbed on top of the Mn atoms in the subsurface, thus favoring the H_2O intercalation on the material.

The OER mechanism was investigated for all the surface terminations, considering bare and OH-covered surfaces. With respect to bare surfaces, the OH bond cleavage – (001) and (011) – and O_2 formation – (111) – are the rate-limiting steps of the reaction. For (001) and (111), the overpotential is higher than 1 V, which indicates that water decomposition is not produced. In addition, the calculated overpotential at surfaces with high Li content is larger than the voltage required for the delithiation process, i.e., the OER is not allowed at these high Li concentrations. Nevertheless, the low lithiated (011) has an overpotential of 0.35 V, being a promising candidate for the OER, and as consequence, a bad candidate as a cathode for aqueous batteries. The computed reaction mechanism for OH-covered surfaces reveals, in general, higher overpotentials than bare surfaces. However, it is worth mentioning that the presence of adsorbed OH moieties favor the formation of the reaction intermediates (*O and *OOH), which are thermodynamically feasible at equilibrium potential (1.23 V). Despite large overpotentials being required to generate O_2, the water decomposition is expected because of the formation of intermediate species on the cathode material. It implies that the surface is covered by reaction intermediates, which may affect the Li intercalation/deintercalation process.

In summary, our DFT study claims the important role of the surface orientation, being the (011) termination with more tendency to lose oxygen and possible catalysts for O_2 generation due to the low overpotential. The formation of oxygen vacancies is not predicted for (001) orientation, although the formation of reaction intermediates at the surface is possible at 1.23 V. The (111) surface shows higher overpotentials for OER.

CRediT authorship contribution statement

Gibu George: Investigation, Formal analysis, Visualization. **Sergio Posada-Pérez:** Conceptualization, Methodology, Investigation, Resources, Data curation, Writing – original draft, Writing – review & editing, Supervision, Funding acquisition. **Albert Poater:** Writing – original draft, Writing – review & editing, Supervision, Funding acquisition, Project administration, Resources. **Miquel Solà:** Writing – original draft, Writing – review & editing, Supervision, Funding acquisition, Project administration, Resources.

Declaration of Competing Interest

The authors declare that they have no known competing financial interests or personal relationships that could have appeared to influence the work reported in this paper.

Data availability

Data will be made available on request.

Acknowledgments

S.P.P. thanks Marie Curie fellowship (H2020-MSCA-IF-2020-101020330). A.P. is a Serra Húnter Professor and thanks ICREA Academia 2019. A.P. and M.S. thank the Spanish Ministerio de Ciencia e Innovación for projects PID2021-127423NB-I00 and PID2020-13711GB-I00 and the Generalitat de Catalunya for project 2017SGR39. Computational time at the *MARENOSTRUM* supercomputer has been provided by the Barcelona Supercomputing Centre through a grant from *Red Española de Supercomputación*. The authors thank Dr. David Santos-Carballal for the surface models.

Appendix A. Supplementary material

Supplementary data to this article can be found online at https://doi.org/10.1016/j.apsusc.2022.155822.

References

[1] A. Manthiram, An outlook on lithium ion battery technology, ACS Cent. Sci. 3 (2017) 1063–1069.
[2] C. Xu, Q. Dai, L. Gaines, M. Hu, A. Tukker, B. Steubing, Future material demand for automotive lithium-based batteries, Commun. Mater. 1 (2020) 99.
[3] H. Kim, J. Hong, K.-Y. Park, H. Kim, S.-W. Kim, K. Kang, Aqueous rechargeable Li and Na ion batteries, Chem. Rev. 114 (2014) 11788–11827.
[4] W. Li, J.R. Dahn, D.S. Wainwright, Rechargeable lithium batteries with aqueous electrolytes, Science 264 (1994) 1115–1118.
[5] L. Smith, B. Dunn, Batteries Opening the window for aqueous electrolytes, Science 350 (2015) 918.
[6] Z. Chang, C. Li, Y. Wang, B. Chen, L. Fu, Y. Zhu, L. Zhang, Y. Wu, W. Huang, A lithium ion battery using an aqueous electrolyte solution, Sci. Rep. 6 (2016) 2.
[7] R. Ruffo, C. Wessells, R.A. Huggins, Y. Cui, Electrochemical behavior of $LiCoO_2$ as aqueous lithium-ion battery electrodes, Electrochem. Commun. 11 (2009) 247–249.
[8] A. Ramanujapuram, D. Gordon, A. Magasinski, B. Ward, N. Nitta, C. Huang, G. Yushin, Degradation and stabilization of lithium cobalt oxide in aqueous electrolytes, Energy Environ. Sci. 9 (5) (2016) 1841–1848.
[9] C. Arbizzani, G. Gabrielli, M. Mastragostino, Thermal stability and flammability of electrolytes for lithium-ion batteries, J. Power Sources 196 (2011) 4801–4805.
[10] Y. Wang, X. Meng, J. Sun, Y. Liu, L. Hou, Recent progress in "water in salt" electrolytes toward non-lithium based rechargeable batteries, Front. Chem. 8 (2020) 595.
[11] H. Tomiyasu, H. Shikata, K. Takao, N. Asanuma, S. Taruta, Y.Y. Park, An aqueous electrolyte of the widest potential window and its superior capability for capacitors, Sci. Rep. 7 (2017) 45048.
[12] F. Wan, J. Zhu, S. Huang, Z. Niu, High-voltage electrolytes for aqueous energy storage devices, Batter. Supercaps 3 (2020) 323–330.
[13] Z.-K. Tang, Y.-F. Xue, G. Teobaldi, L.-M. Liu, The oxygen vacancy in Li-ion battery cathode materials, Nanoscale Horiz. 5 (2020) 1453–1466.
[14] R. Hausbrand, G. Cherkashinin, H. Ehrenberg, M. Gröting, K. Albe, C. Hess, W. Jaegermann, Fundamental degradation mechanisms of layered oxide Li-ion battery cathode materials: Methodology, insights and novel approaches, Mater. Sci. Eng. B 192 (2015) 3–25.
[15] S. Lee, W. Jin, S.H. Kim, S.H. Joo, G. Nam, P. Oh, Y.-K. Kim, S.K. Kwak, J. Cho, Oxygen vacancy diffusion and condensation in lithium-ion battery cathode materials, Angew. Chem. Int. Ed. 58 (2019) 10478–10485.
[16] S. Sharifi-Asl, J. Lu, K. Amine, R. Shahbazian-Yassar, Oxygen release degradation in Li-ion battery cathode materials: mechanism and mitigating approaches, Adv. Energy Mater. 9 (2019) 1900551.
[17] S. Posada-Pérez, G. Hautier, G.M. Rignanese, Effect of aqueous electrolytes on $LiCoO_2$ surfaces: role of proton adsorption on oxygen vacancy formation, J. Phys. Chem. C 126 (2022) 110–119.
[18] Y. Hinuma, T. Toyao, T. Kamachi, Z. Maeno, S. Takakusagi, S. Furukawa, I. Takigawa, K.-I. Shimizu, Density functional theory calculations of oxygen vacancy formation and subsequent molecular adsorption on oxide surfaces, J. Phys. Chem. C 122 (2018) 29435–29444.
[19] W. Hu, H. Wang, W. Luo, B. Xu, C. Ouyang, Formation and thermodynamic stability of oxygen vacancies in typical cathode materials for Li-ion batteries: density functional theory study, Solid State Ion. 347 (2020) 115257.
[20] L. Suo, O. Borodin, T. Gao, M. Olguin, J. Ho, X. Fan, C. Luo, C. Wang, K. Xu, "Water-in-Salt" electrolyte enables high-voltage aqueous lithium-ion chemistries, Science 350 (2015) 938–943.
[21] L. Suo, O. Borodin, Y. Wang, X. Rong, W. Sun, X. Fan, S. Xu, M.A. Schroeder, A. V. Cresce, F. Wang, C. Yang, Y.S. Hu, K. Xu, C. Wang, "Water-in-Salt" electrolyte makes aqueous sodium-ion battery safe, green, and long-lasting, Adv. Energy Mater. 7 (2017) 21.
[22] J. Vatamanu, O. Borodin, Ramifications of water-in-salt interfacial structure at charged electrodes for electrolyte electrochemical stability, J. Phys. Chem. Lett. 8 (2017) 4362–4367.
[23] X. Guo, Z. Wang, Z. Deng, B. Wang, X. Chen, S.P. Ong, Design principles for aqueous Na-ion battery cathodes, Chem. Mater. 32 (2020) 6875–6885.
[24] R.K. Guduru, J.C. Icaza, A brief review on multivalent intercalation batteries with aqueous electrolytes, Nanomaterials 6 (2016) 41.
[25] D. Chao, W. Zhou, F. Xie, C. Ye, H. Li, M. Jaroniec, S.Z. Qiao, Roadmap for advanced aqueous batteries: from design of materials to applications, Sci. Adv. 6 (2020) eaba4098.
[26] W. Tang, Y. Zhu, Y. Hou, L. Liu, Y. Wu, K.P. Loh, H. Zhang, K. Zhu, Aqueous rechargeable lithium batteries as an energy storage system of superfast charging, Energy Environ. Sci. 6 (2013) 2093–2104.
[27] S. Chen, S.R. Jeong, S. Tao, Key materials and future perspective for aqueous rechargeable lithium-ion batteries, Mater. Rep. Energy 2 (2022), 100096.
[28] J. Yun, R. Sagehashi, Y. Sato, T. Masuda, S. Hoshino, H.B. Rajendra, K. Okuno, A. Hosoe, A.S. Bandarenka, N. Yabuuchi, Nanosized and metastable molybdenum oxides as negative electrode materials for durable high-energy aqueous Li-ion batteries, Proc. Natl. Acad. Sci. U. S. A. 118 (2021) e2024969118.
[29] S. Park, S. Okada, J. Yamaki, Symmetric cell with $LiMn_2O_4$ for aqueous lithium-ion battery, J. Nov. Carbon Resour. Sci. 3 (2011) 27–31.
[30] Y.S. Choe, C.J. Kang, An electrostatic potential study of $LiMn_2O_4$ cathode material for lithium-ion battery: an insight into Li^+ ion migration channels, Phys. B Condens. Matter 640 (2022), 414044.
[31] H. Seki, K. Yoshima, Y. Yamashita, S. Matsuno, N. Takami, Aqueous lithium-ion battery of $Li_4Ti_5O_{12}/LiMn_2O_4$ using a lithium-ion conductive solid electrolytes separator, J. Power Sources 482 (2021), 228950.
[32] K. Nakajima, F.L. Souza, A.L.M. Freitas, A. Thron, R.H.R. Castro, Improving thermodynamic stability of nano-$LiMn_2O_4$ for Li-ion battery cathode, Chem. Mater. 33 (2021) 3915–3925.
[33] J. Shin, J.K. Seo, R. Yaylian, A. Huang, Y.S. Meng, A review on mechanistic understanding of MnO_2 in aqueous electrolyte for electrical energy storage systems, Int. Mater. Rev. 65 (2020) 356–387.
[34] W. Tang, S. Tian, L.L. Liu, L. Li, H.P. Zhang, Y.B. Yue, Y. Bai, Y.P. Wu, K. Zhu, Nanochain $LiMn_2O_4$ as ultra-fast cathode material for aqueous rechargeable lithium batteries, Electrochem. Commun. 13 (2011) 205–208.
[35] L. Tian, A. Yuan, Electrochemical performance of nanostructured spinel $LiMn_2O_4$ in different aqueous electrolytes, J. Power Sources 192 (2009) 693–697.
[36] M. Kheirmand, A. Ghasemi, $LiMn_2O_4$ nanoparticles as cathode in aqueous lithium-ion battery, Surf. Eng. Appl. Electrochem. 52 (2016) 480–486.
[37] Y. Wen, C. Ma, H. Chen, H. Zhang, M. Li, P. Zhao, J. Qiu, H. Ming, G. Cao, G. Tang, Stabilizing $LiMn_2O_4$ cathode in aqueous electrolyte with optimal concentration and components, Electrochim. Acta 362 (2020), 137079.
[38] W. Pei, Y. Hui, Y. Huaquan, Electrochemical behavior of Li-Mn spinel electrode material in aqueous solution, J. Power Sources 63 (1996) 275–278.
[39] R. Sharpe, R.A. House, M.J. Clarke, D. Förstermann, J.-J. Marie, G. Cibin, K.-J. Zhou, H.Y. Playford, P.G. Bruce, M.S. Islam, Redox chemistry and the role of trapped molecular O_2 in Li-rich disordered rocksalt oxyfluoride cathodes, J. Am. Chem. Soc. 142 (2020) 21799–21809.
[40] K.Y. Lin, S. Nachimuthu, H.W. Huang, J.C. Jiang, Theoretical insights on alleviating lattice-oxygen evolution by sulfur substitution in $Li_{1.2}Ni_{0.6}Mn_{0.2}O_2$ cathode material, npj Comput. Mater. 8 (2022) 210.
[41] S. Sharifi-Asl, J. Lu, K. Amine, R. Shahbazian-Yassar, Oxygen release degradation in Li-ion battery cathode materials: mechanisms and mitigating approaches, Adv. Energy Mater. 9 (2019) 1900551.
[42] X. Gao, Y.H. Ikuhara, C.A.J. Fisher, R. Huang, A. Kuwabara, H. Moriwake, K. Kohama, Y. Ikuhara, Oxygen loss and surface degradation during electrochemical cycling of lithium-ion battery cathode material $LiMn_2O_4$, J. Mater. Chem. A 7 (2019) 8845–8854.
[43] L. Ben, H. Yu, B. Chen, Y. Chen, Y. Gong, X. Yang, L. Gu, X. Huang, Unusual spinel-to-layered transformation in $LiMn_2O_4$ cathode explained by electrochemical and thermal stability investigation, ACS Appl. Mater. Interfaces 9 (2017) 35463–35475.
[44] J. Choi, E. Alvarez, T.A. Arunkumar, A. Manthiram, Proton insertion into oxide cathodes during chemical delithiation, Electrochem. Solid St. 9 (2006) A241.
[45] R. Benedek, M.M. Thackeray, A. van de Walle, Free energy for protonation reaction in lithium-ion battery cathode materials, Chem. Mater. 20 (2008) 5485–5490.
[46] J.Y. Luo, Y.Y. Xia, Aqueous lithium-ion battery $Li_4Ti_2(PO_4)_3/LiMn_2O_4$ with high power and energy densities as well as superior cycling stability, Adv. Funct. Mater. 17 (2007) 3877–3884.
[47] S. Posada-Pérez, G.M. Rignanese, G. Hautier, Influence of stacking on H^+ intercalation in layered $ACoO_2$ (A= Li, Na) cathode materials and implications for aqueous Li-ion batteries: a First-principles investigation, Chem. Mater. 33 (2021) 6942–6954.

[48] A. Abbaspour-tamijani, J.W. Bennett, D.T. Jones, Z.R. Jones, E.D. Laudadio, J. Robert, J.A. Santana, S.E. Mason, DFT and thermodynamic calculations of surface cation release in $LiCoO_2$, Appl. Surf. Sci. 515 (2020), 145865.
[49] J.W. Bennett, D. Jones, X. Huang, R.J. Hamers, S.E. Mason, Dissolution of complex metal oxides from first-principles and thermodynamics: cation removal from the (001) surface of $Li(Ni_{1/3}Mn_{1/3}Co_{1/3})O_2$, Environ. Sci. Tech. 52 (2018) 5792–5802.
[50] Y.S. Meng, M.E. Arroyo-de Dompablo, Recent advances in first-principles computational research of cathode materials for lithium-ion batteries, Acc. Chem. Res. 46 (2013) 1171–1180.
[51] Y.S. Meng, M.E. Arroyo-De Dompablo, First principles computational materials design for energy storage materials in lithium ion batteries, Energ. Environ. Sci. 2 (2009) 589–609.
[52] A. Urban, D.H. Seo, G. Ceder, Computational understanding of Li-ion batteries, npj Comput. Mater. 2 (2016) 16002.
[53] G. Kresse, J. Furthmüller, Efficient iteratives schemes for ab initio total-energy calculations using plane-wave basis set, Phys. Rev. B: Condens. Matter Mater. Phys. 54 (1996) 11169.
[54] J.P. Perdew, K. Burke, M. Ernzerhof, Generalized gradient approximation made simple, Phys. Rev. Lett. 77 (1996) 3865.
[55] S. Grimme, J. Anthony, S. Ehrlich, H. Krieg, A consistent and accurate ab initio parametrization of density functional dispersion correction (DFT-D) for the 94 elements H-Pu, J. Chem. Phys. 132 (2010), 154104.
[56] B. Ramogayana, D. Santos-Carballal, P.A. Aparicio, M.G. Quesne, K.P. Maenetja, P. E. Ngoepe, N.H. de Leeuw, Ethylene carbonate adsorption on the major surfaces of lithium manganese oxide $Li_{1-x}Mn_2O_4$ spinel: a DFT+U D3 study, Phys. Chem. Chem. Phys. 22 (2020) 6763–6771.
[57] S. Dudarev, G. Botton, Electron-energy-loss spectra and the structural stability of nickel oxide: an LSDA +U study, Phys. Rev. B: Condens. Matter Mater. Phys. 57 (1998) 1505.
[58] P.E. Blöchl, Projector augmented wave method, Phys. Rev. B 50 (24) (1994) 17953–17979.
[59] G. Kresse, D. Joubert, From ultrasoft pseudopotentials to the projector augmented-wave method, Phys. Rev. B 59 (1999) 1758.
[60] H.J. Monkhorst, J.D. Pack, Special points for Brillouin-zone integrations, Phys. Rev. B: Solid State 13 (1976) 5188.
[61] G.W. Watson, E.T. Kelsey, N.H. de Leeuw, D.J. Harris, S.C. Parker, Atomistic simulations of dislocations, surfaces and interfaces in MgO, J. Chem. Soc. Faraday Trans. 92 (1996) 433–438.
[62] P.W. Tasker, The stability of ionic crystal surfaces, J. Phys. C Solid State Phys. 12 (1979) 4977–4984.
[63] R. Benedeck, M.M. Thackeray, Simulation of the surface structure of lithium manganese oxide spinel, Phys. Rev. B 83 (2011), 195439.
[64] A. Karim, S. Fosse, K.A. Persson, Surface structure and equilibrium particle shape of the $LiMn_2O_4$ spinel from first-principles calculations, Phys. Rev. B 87 (2013), 075322.
[65] R.E. Warburton, H. Iddir, L.A. Curtiss, J. Greeley, Thermodynamic stability of low- and high-index spinel $LiMn_2O_4$ surface terminations, ACS Appl. Mater. Interfaces 8 (2016) 11108–11121.
[66] C.Y. Ouyang, X.M. Zeng, Z. Sljivancanin, A. Baldereschi, Oxidation states of Mn atoms at clean and Al_2O_3-covered $LiMn_2O_4$ (001) surface, J. Phys. Chem. C 114 (2010) 4756–4759.
[67] M.M. Thackeray, M.F. Mansuetto, J.B. Bates, Structural stability of $LiMn_2O_4$ electrodes for lithium batteries, J. Power Sources 68 (1997) 153–158.
[68] I.C. Man, H.Y. Su, F. Calle-Vallejo, H.A. Hansen, J.I. Martínez, N.G. Inoglu, J. Kitchin, T.F. Jaramillo, J.K. Nørskov, J. Rossmeisl, Universality of oxygen evolution electrocatalysis on oxide surfaces, ChemCatChem 3 (2011) 1159–1165.
[69] Q. Liang, G. Brocks, A. Bieberle-Hütter, Oxygen evolution reaction (OER) mechanism under alkaline and acidic conditions, J. Phys. Energy 3 (2021), 026001.
[70] J.K. Nørskov, J. Rossmeisl, A. Logadottir, L. Lindqvist, J.R. Kitchin, T. Bligaard, H. Jónsson, Origin of the overpotential for oxygen reduction at fuel-cell cathode, J. Phys. Chem. B 108 (2004) 17886–17892.
[71] K. Leung, L.C. Merrill, K.L. Harrison, Galvanic corrosion and electric field in lithium anode passivation films: effects on self-discharge galvanic corrosion and electric field in lithium anode passivation films: effects on self-discharge, J. Phys. Chem. C 126 (20) (2022) 8565–8580.
[72] C. Wang, A.C. Thenuwara, J. Luo, P.P. Shetty, M.T. McDowell, H. Zhu, S. Posada-Perez, H. Xiong, G. Hautier, W. Li, Extending the low-temperature operation of sodium metal batteries combining linear and cyclic ether-based electrolyte solutions, Nat. Commun. 13 (2022) 4934.
[73] J. Zheng, Y. Hou, Y. Duan, X. Song, Y. Wei, T. Liu, J. Hu, H. Guo, Z. Zhuo, L. Liu, Z. Chang, X. Wang, D. Zherebetskyy, Y. Fang, Y. Lin, K. Xu, L.-W. Wang, Y. Wu, F. Pan, Janus Solid-liquid interface enabling ultrahigh charging and discharging rate for advanced lithium-ion batteries, Nano Lett. 15 (2015) 6102–6109.
[74] J. Hu, W. Ren, X. Chen, Y. Li, W. Huang, K. Yang, L. Yang, Y. Lin, J. Zheng, F. Pan, The role of anions on the Helmholtz plane for the solid-liquid interface in aqueous rechargeable lithium batteries, Nano Energy 74 (2020), 104864.
[75] D. Kramer, G. Ceder, Tailoring the morphology of $LiCoO_2$: a first principles study, Chem. Mater. 21 (2009) 3799–3809.
[76] V. Tripković, E. Skúlason, S. Siahrostami, J.K. Nørskov, J. Rossmeisl, The oxygen reduction reaction mechanism on Pt(111) from density functional calculations, Electrochim. Acta 55 (2010) 7975–7981.